Modeling the Active-Site Structure of the *cbb*$_3$-Type Oxidase from *Rhodobacter sphaeroides*[†]

Vivek Sharma, Mårten Wikström, and Liisa Laakkonen*

Helsinki Bioenergetics Group, Programme for Structural Biology and Biophysics, Institute of Biotechnology, University of Helsinki, Helsinki 00014, Finland

Received October 17, 2007; Revised Manuscript Received January 10, 2008

ABSTRACT: The active site of the heme−copper oxidases comprises a redox-active high-spin heme and a tris-histidine copper center Cu_B. Two amino acids in the close vicinity of the metals, a tyrosine and a tryptophan from helix 6, have been shown to be absolutely required for the catalytic function and should be considered part of the active site. Additionally, amino acid residues from interhelical loops strongly modify the activity. In a separate subfamily of heme−copper oxidases, the *cbb*$_3$-type oxidases, the metal centers are identical, the tyrosine is found in helix 7, but nothing is known of the corresponding tryptophan or of the involvement of the loop residues. We have observed a conserved aromatic cluster in the known oxidase structures, including the essential tryptophan and loop residues, and refined our earlier model of the *cbb*$_3$-type oxidase from *Rhodobacter sphaeroides* to test the feasibility of a similar structure. In the refined model, the interactions around the Δ-propionate of the high-spin heme resemble closely those seen in crystal structures of other terminal oxidases. Two alternative models (G- and C-models) that differ for the positioning of conserved tryptophans in helix 6, are presented. Molecular dynamics simulations on the catalytic subunit of the *cbb*$_3$-type oxidase model result in a conformational change of the active-site tyrosine, which may be related to different ligand-binding properties of the *cbb*$_3$-type oxidases. The relationship between sequence and functional data for defining the subfamily is discussed.

The superfamily of heme−copper oxidases can be defined by the structure of the active site: two hemes and a copper atom, seven invariant histidines ligating them, and a redox-active tyrosine residue covalently bound to one of the copper ligands. The tyrosine is a key residue for the catalysis, donating an electron and a proton for the first steps of oxygen reduction chemistry (*1*). Recent data suggest a similar role for a tryptophan that stacks to another of the copper atom of the binuclear site (Cu_B)[1] ligating histidines (B:W236 and B:H291, residue numbers for the *aa*$_3$-type oxidases are from the subunit I of the *Bos taurus* enzyme, unless specifically mentioned) (*2, 3*). Catalysis occurs between the two transition metals, central iron of the high-spin heme (Fe_{a3}) and Cu_B, within the transmembraneous protein, and the four electrons and four protons needed to reduce O_2 to water are fed in via other redox centers in the protein and water-filled channels, respectively (*4, 5*). The vectorial chemistry itself generates a transmembrane electrochemical gradient, and the large reaction energy is converted to translocation of four more protons across the membrane.

All aerobic organisms have one or more terminal oxidases, which can be quite divergent on the level of primary structure, even though the reaction catalyzed is identical. A separate subfamily is formed by the *cbb*$_3$-type oxidases, defined by a unique subunit composition, three C-type hemes in the noncatalytic subunits, two B-type hemes in the central subunit (*6, 7*), and the transfer of the catalytic tyrosine from helix 6 to helix 7 (*8–11*). The sequence identity of the catalytic subunit of the *cbb*$_3$-type oxidase from *Rhodobacter sphaeroides* is equally low (∼20%) compared to all structurally resolved cytochrome *c* oxidases. There are also numerous oxidase sequences from genomic projects that resemble the *cbb*$_3$-type oxidases in having the conserved tyrosine in helix 7 (*12*). Their sequence identity to the functionally characterized representatives of the cytochrome *cbb*$_3$ subfamily varies down to 20–30% (see below), and the metabolism of many of these aberrant organisms from highly variant environments is unknown. Our goal is to understand the structure and the catalytic mechanism of the *cbb*$_3$-type oxidase from *R. spaheroides*, and as long as the largely divergent *cbb*$_3$-like proteins have not been shown to function similarly (e.g., act as proton pumps and not as oxygen scavengers only), we consider the sequence data interesting in a phylogenetic sense but not binding in studying mechanistic details.

In the crystal structures of *aa*$_3$, *bo*$_3$, and *ba*$_3$ oxidases, the fully conserved tryptophan in helix 6 (B:W236) stacks to one of the histidines ligating Cu_B (B:His291). In addition, the opposite face of the tryptophan interacts with the residue before it, B:F235, and the aromatic chain continues further to B:W126 in loop 3–4. Mutation of the corresponding

[†] The work was supported by the Academy of Finland, the Sigrid Jusélius Foundation, and Biocentrum Helsinki.

* To whom correspondence should be addressed: P.O. Box 56, Viikinkaari 4, University of Helsinki, Helsinki 00014, Finland. Telephone: +358-9-191-57625. Fax: +358-9-191-57620. E-mail: liisa.laakkonen@helsinki.fi.

[1] Abbreviations: COX, cytochrome *c* oxidase; NOR, nitric oxide reductase; PDB, Protein Data Bank; Cu_B copper atom of the binuclear site; Fe_{a3} central iron of the high-spin heme; B, subunit I of the cytochrome *c* oxidase from *Bos taurus*.

10.1021/bi702088r CCC: $40.75
Published on Web 03/14/2008

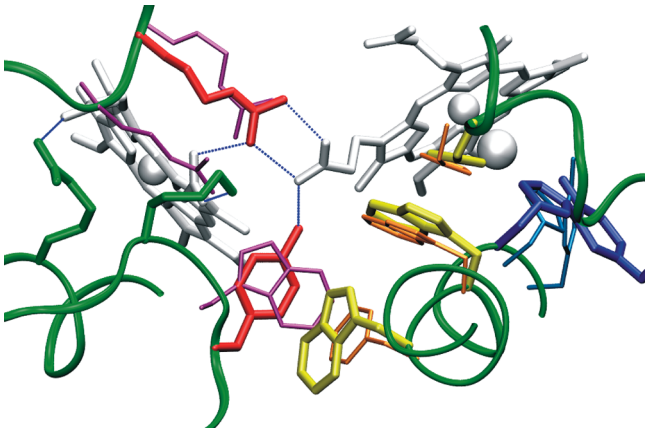

FIGURE 1: Superposition of the active sites of the model of the cbb_3-type oxidase (in thick lines) and the bovine aa_3-type oxidase (in thin lines) viewed from above the hemes. Hemes and Cu_B are shown in silver, with the low-spin heme on the left and the binuclear center on the right. Backbone ribbons for helix 2, loop 3–4, helix 6, helix 7, and loop 11–12 are shown in green, counted counter-clockwise from the lower left corner. Three areas of of interest are highlighted: the competing hydrogen bonds with the high-spin Δ-propionate in red/purple (cbb_3, Y181 and R471; aa_3, W126 and R438), the aromatic cluster in yellow/orange (cbb_3, W263, W264, and H318; aa_3, F235, W236, and H291), and the His−Tyr pair in blue/cyan (cbb_3, H267 and Y311; aa_3, H240 and Y244). Ligands of the low-spin heme *b*, R115 and K179, are shown in green. This model has been constructed from the gapped alignment.

tryptophan to a phenylalanine in the *Paracoccus denitrificans* aa_3-type oxidase renders the enzyme completely inactive (*2*). The possible importance of the connection between two fully conserved aromatics is not known. Helix 6 of the cbb_3-type oxidases has instead two consecutive conserved tryptophans, either of which could form a similar interaction with the copper ligand. Here, we have modeled both alternative positions of the tryptophans separately (G- and C-models).

Electronic properties of heme groups are modified by the interactions that they form with the environment, particularly, via their charged propionate groups. In the known crystal structures, each heme propionate is involved in polar interactions with well-conserved residues in the loops between transmembrane helices 3 and 4, 9 and 10, and 11 and 12 (*13–19*) (see Figure 1), and several of these have been shown to be central in the function of the enzyme (*20–22*). The loop between helices 3 and 4 (loop 3–4) differs intriguingly in the cbb_3-type oxidases from the corresponding one in the aa_3-type oxidases. However, the segment is well-conserved within each subfamily: gtg**W**tv**Y**ppla in the aa_3-type oxidases and ke**Y**ae in the cbb_3-type oxidases (residues discussed in detail are shown in bold). The two aromatic residues of the aa_3-type oxidases, B:Trp126 and B:Tyr129, form conserved interactions within the protein: B:W126 forms a hydrogen bond to the Δ-propionate of the high-spin heme and B:Y129 to B:W236 in helix 6. The corresponding residues have been mutated to phenylalanines in the aa_3-type oxidase from *P. denitrificans*, and the mutants exhibit about half of the wild-type catalytic activity: W → F at 40% (*22*) and Y → F at 60% (*23*). In all resolved structures, the Δ-propionate of the high-spin heme also interacts with B:R438 from the loop between helices 11 and 12 (loop 11–12), and the competition between the two polar interactions is proposed to be part of the mechanism by which the proton and water exit are gated (*24, 25*). The mutation of the analogous arginine to several different residues in *Escherichia coli* bo_3 oxidase and *R. sphaeroides* aa_3 oxidase verifies its importance for activity and proton pumping in these enzymes (*20, 21*).

The single aromatic residue in loop 3–4 of the cbb_3-type oxidases, Y181, could *a priori* match either B:W126 or B:Y129. In our first cbb_3 model (*9*), B:Y129 was chosen to be the counterpart of Y181 mainly because the shorter loop 3–4 of the cbb_3-type oxidases covers better the longer ones of the template structures and allows for a full-length transmembrane helix 4 from P184 onward. Fixing the position of Y181 in the model was followed by a spatial corollary: the counterion for the Δ-propionate would need to be K179 from loop 3–4, and then the opposite residue is necessarily the fully conserved W470 from loop 11–12. This way, the interactions provided by the two loops were inverted, and the aromatic residue of the triad K179−Δ-prp_{b3}−W470 is not on the same side of the hemes as helix 6 but located in loop 11–12.

We have now remodeled the active site of the cbb_3-type oxidase from *R. sphaeroides*, by matching Y181 to B:W126. The resulting arrangement closely resembles the crystal structures of oxidases and allows for the formation of an analogous extended aromatic structure between helix 6 and loop 3–4. The detailed model of the active site shows that, despite major differences at the level of primary structure, the atomic interactions between the redox centers and the protein may be very similar in the oxidase subfamilies.

MATERIALS AND METHODS

Homology models of the cbb_3-type oxidase from *R. sphaeroides* were produced with the program MODELLER7v7 (*26*), as described earlier (*9*), and the structures were visualized for analysis with the program Visual Molecular Dynamics (VMD) (*27*). Multiple sequence alignments were generated with ClustalX1.8 (*28*), and they are the same as used previously (*9*), with minor manual changes performed in helix 6 and loop 3–4/11–12 (see below). BioEdit (*29*) was used for additional sequence analysis. The sequence to be modeled was gi: 1377865 (*6*), and the structural templates Protein Data Bank (PDB) 1V55 (*B. taurus*) and 1EHK (*Thermus thermophilus*). The prehelix was omitted from the construction (residues 1–64 of the target sequence).

Y181 and R471 of the target sequence were manually aligned to the W126/Y133 and R438/R449, respectively, of the template sequences from *B. taurus*/*T. thermophilus*. Similarly for the alternative model, W263W264 were aligned to F235W236/F228W229 by introducing a gap in the alignment (see the Discussion). MODELLER extracts almost the same initial atomic coordinates for a residue in the target sequence, when the residue in the template sequence at an equivalent position is the same. Therefore, no explicit MODELLER restraints were needed for enforcing those residue positions. However, the interactions, which were forced using distance restraints of MODELLER, are as follows: (H267/NE2−Y311/CE2), (K179/NZ−low-spin heme *b*/O1D), (R115/NH2−E472/O), and (R115/NH1−low-spin heme *b*/O1A). α restraints of MODELLER were invoked, at the positions of intrahelical insertions or deletions in the alignment, and a six-residue surface helix was constructed in loop 11–12. The two water molecules

(a)

```
                helix3hhhhh------------loop3-4------------hhelix4h
Bos taurus      PPSFLLLLASSMVEA-----GAGTGWTVYPPLAGNLAHAG--ASVDLTIF
P.denitr.aa3    VCGVALGVASLLAPGGNDQMGSGVGWVLYPPLS--TTEAG--YSMDLAIF
T.thermo.ba3    FIGLVVAALPLLA---N---EATVLYTFYPPLK---------GHWAFYL
R.sph. cbb3     NLFIVLVAQSYLLGAT----QSKE-Y-------------AE-----PEW
```

(b)

```
                ----hhhhhhhhhhhh-helix6-hhhhhhhhhhhhhhh--------hhh
Bos taurus      GGGDPILYQHLFWFFGHPEVYILILPGF-GMISHIVTYYSGK-KEPFGYM
P.denitr.aa3    GGGDPVLYQHILWFFGHPEVYIIILPGF-GIISHVISTFAKK--PIFGYL
T.thermo.ba3    EGVDPLVARTLFWWTGHPIVYFWLLPAY-AIIYTILPKQAGG--KLVSDP
R.sph. cbb3C    ----GVQDAMVQWWYGHNAVGFFLTAGFLGMMYYFVPKQAE--RPVYSYK
R.sph. cbb3G    ---GVQDAMVQWW-YGHNAVGFFLTAGFLGMMYYFVPKQAE--RPVYSYK
```

(c)

```
                hhhhhhelix11hhhhhhhhh---loop11-12-----------hhhhh
Bos_taurus      IHFAIMFVGVNMTFFPQHFLG-LSGM-PRRYSDYP----------DAYT
P.denitr.aa3    LHFWMMFIGSNLIFFPQHFLG-RQGM-PRRYIDYP----------VEFA
T.thermo.ba3    AVVWLWFLGMMIMAVGLHWAG-LLNV-PRRAYIAQVP------DAYPHAA
R.sph. cbb3     WHFWLATIGIVLYASSMWVSGIMEGLMWREVDANGFLVNA-FADTVAAKF
```

FIGURE 2: Modified alignment for (a) loop 3–4, (b) helix 6, and (c) loop 11–12. Bt stands for *B. taurus*; Pd stands for *P. denitrificans*; and Tt stands for *T. thermophilus*.

between the heme propionates were modeled explicitly from the template structures. After the same modeling procedure was used as before (*9*), 5 models with the lowest value of the MODELLER objective function were selected for refinement and analysis of 50 models generated.

Water molecules were added to the selected models using DOWSER (*30*). The energy cutoff for DOWSER was −10 kcal/mol. The hydrated system was relaxed with 2000 steps of unconstrained conjugate gradient minimization in NAMD/VMD (*31*), followed by molecular dynamics simulation. The Cα atoms were kept under harmonic constraints of 10 kcal mol^{-1} Å^{-2}, to compensate for missing subunits and the membrane/water environment. The simulations were carried out for 450 ps, with a time step of 1 fs. Langevin dynamics was used to keep a constant temperature of 300 K. The trajectory was saved every picosecond. Control simulations were performed with an identical protocol for the catalytic subunit of the bovine enzyme.

Calculations were performed with the CHARMM27 force field (*32*). For A-type hemes and the $Cu_B(His)_3$ center, newly developed charges (*33*) were used with in-house-developed parameters, while in-house-developed topology and parameters were used for B-type hemes. For the covalently bound histidine−tyrosine pair, a patch residue was constructed to reproduce the experimental geometry. Analysis of simulations and trajectories was performed with VMD and Xmgrace (http://plasma-gate.weizmann.ac.il/Grace/).

RESULTS

Refined molecular models of the *cbb*$_3$-type oxidase from *R. sphaeroides* were constructed from the slightly modified alignment shown in Figure 2. Figure 1 shows a comparison of the active site between the model and the bovine structure. Specifically, Y181 and R471 of the target sequence were aligned to match W126/Y133 and R438/R449 of the bovine/*T. thermophilus* enzyme, and the interactions listed in the Materials and Methods were constrained to form. For helix 6, two alternatives were considered. In the first case, the sequence was kept continuous as before (model C), and in the second case, a gap (model G) was inserted after W264 and the helix was constrained to stay straight. In model G, an extended aromatic cluster is formed between H318, W264, W263, and Y181. Most of the applied distance restraints (see the Materials and Methods) were found satisfied in the selected models, which were optimized smoothly and appeared physically reasonable by visual inspection. The coordinates of the updated models can be obtained upon request (liisa.laakkonen@helsinki.fi). The interactions of each heme propionate with protein residues are listed in Table 1.

Table 1: Comparison of Interactions of Heme Propionates in the Bovine Crystal Structure and the *R. sphaeroides cbb*$_3$ Model[a]

heme	propionate	*B. taurus*/*aa*$_3$	*R. sphaeroides* model/*cbb*$_3$
a/*b*	O1A	Y54/OH, Y371/OH, w	R115/NH1
	O2A	R439/N, w	E472/N
	O1D	W126/N	Y181/N
	O2D	R439/NE, w	K179/NZ
a$_3$/*b*$_3$	O1A	D364/OD2, H368/ND1	N393/ND2,H397/ND1
	O2A	H368/ND1, w, w	H397/ND1
	O1D	R438/NH1, w, w	R471/NH1
	O2D	R438/NH2, W126/NE1	R471/NH2, Y181/OH

[a] An interacting water molecule is marked with a w.

At minimization and simulation, Y311 of the His−Tyr pair relaxes to a different conformation than in the templates, while the internal geometry of the dimer stays intact during 450 ps of simulation. The average χ_2 dihedral angle of tyrosine, the interplanar angle, and the improper torsion of the His−Tyr pair ($C\epsilon1_{His267}-C\epsilon2_{Tyr311}-N\epsilon2_{His267}-C\delta2_{His267}$) are 154°, −39°, and 162° for the *cbb*$_3$-type oxidase model. The corresponding values for the bovine enzyme are −83°, 68°, and 165°. The distance for $O_{Y311}-Cu_B$ is 5.1 Å, and the distance for $O_{Y311}-Fe$ is 4.8 Å in the homology model, while in crystal structure of bovine oxidases, the distance for $O_{Y244}-Cu_B$ is 5.7 Å and the distance for $O_{Y244}-Fe$ is 5.7 Å. The triplet interaction between R471, the Δ-propionate of the high-spin heme, and Y181 in the model remains stable during the 450 ps simulation.

The alignment of the 246 *cbb*$_3$-like sequences from Hemp et al. (*12*) was analyzed further. The four well-studied *cbb*$_3$ enzymes from *Bradyrhizobium japonicum*, *R. sphaeroides*, *Rhodobacter capsulatus*, and *Vibrio cholerae* were compared to each sequence in the complete data set from the given alignment, and the pairwise identities are shown in Figure 3. A value of 100% is reached when the sample sequence is compared to itself. The overall behavior is the same for each of the four sequences studied. First, there are 17 sequences that are 50–60% identical to each of the four. Then, the comparison moves to the sequence space where all four sample sequences originate, and the identities rise abruptly to over 60%. In this interval, each of the four sample sequences shows variable values, reflecting relationships between the bacteria. At sequence 191, the identity scores drop steeply. For the last two phases of the curve, the four sample sequences again show similar values, first at identity levels around 40% and then below 30%. We conclude that 173 sequences (from 18 to 191; Figure 3) form an internally highly similar set, which we consider relevant for functional comparisons, as all available data originates from this set. In this set, loop 3–4 residues E180 and Y181 are fully conserved, as are W263 and W264 from helix 6. K179 is

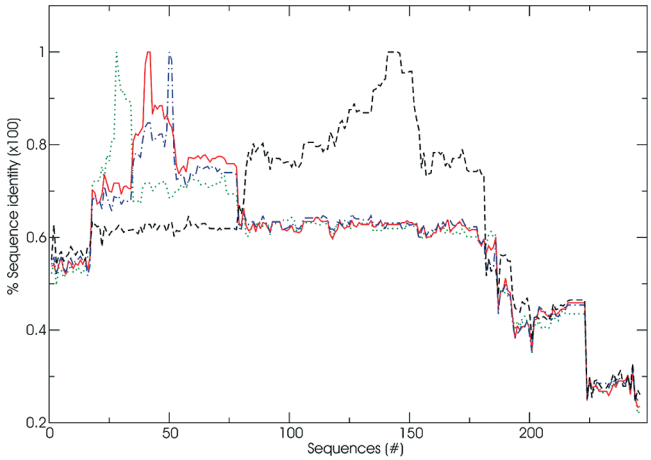

FIGURE 3: Sequence comparison of the four functionally charaterized cbb_3-type oxidases to the large data set. The percent identity of *B. japonicum* sequence to each of the 246 sequences is shown as a green dotted line; the percent identity of *R. sphaeroides* sequence to each of the 246 sequences is shown as a red solid line; the percent identity of *R. capsulatus* sequence to each of the 246 sequences is shown as a blue dash-dotted line; and the percent identity of *V. cholerae* sequence to each of the 246 sequences is shown as a black dashed line.

often replaced by R, 3 times by Q, and 1 time by L. R471 is replaced 1 time by G, 4 times by S, 6 times by L, and 1 time by Q. Given the functional role assigned to K179 in our models and the experimental data on corresponding sites in the aa_3-type oxidases (*20, 21*), substitution of K179 by R or Q should be functionally accepted and only the single substitution by a leucine should be considered a problem (172/173 = 99% conserved). For R471 as the cation in the arginine−propionate pair, all 12 substitutions listed are unacceptable and the site appears variable even in this smaller set of sequences (161/173 = 93% conserved).

DISCUSSION

Structural modeling of the cbb_3-type oxidases is challenging because of the low sequence identity within the superfamily and the very high sequence identity among the cbb_3 oxidases themselves (>60%, see Figure 3.) Each of the three segments discussed here, loop 3–4, helix 6, and loop 11–12, align unambiguously, fully gaplessly, within the cbb_3 oxidases, but the conserved residues in them (K179E180Y181, W263W264, and W470R471) can be aligned in alternative ways to the known crystal structures. Especially for the loop areas, the different alignments cannot be discriminated by structural or bioinformatic arguments. What can be done, though, is to constract models from the alignments and compare them to the crystal structures, where these three segments are linked together via contacts to the hemes. The number of structural alternatives in modeling is limited by the residues studied, being so close to each other in the primary sequence and by the fully rigid arrangement of the hemes; assigning a structural role to one residue severely restricts possiblities for the others.

Old versus Refined Model. Our earlier model was based on matching Y181 to B:Y129, for reasons given in the introduction, and roles for the other residues in loops 3–4 and 11–12 followed from this. Since then, new data on the critical role of the conserved tryptophan in helix 6 (B:W236) has been published (*3*). In the known oxidase structures, this tryptophan stacks to one of the histidine ligands of the CuB center (see Figure 1), and moreover, it is central in an cluster of tightly packed hydrophobic residues extending up to the aromatic residue of the propionate triad. We wanted now to revisit the assignment of Y181 and study the possibility of keeping the aromatic residue on the same side of the hemes as helix 6, thus allowing for the formation of an analogous hydrophobic structure. This assigns Y181 to B:W126, in close resemblance to the ba_3-type oxidases, where a tyrosine, not a tryptophan, serves as the aromatic residue in the triad (*14*). Sterically, it is not possible for both next-to-neighbors Y181 and K179 to interact with the same propionate, but the basic residue has to reside elsewhere. We assigned this role to the sole arginine in loop 11–12 of the cbb_3-type oxidases and matched it to the first of the two consecutive arginines in the aa_3-type oxidases (see Figure 2). The competing interactions within the triad Y181−Δ-prp$_{b3}$−R471 are now fully analogous to the configuration observed in the crystal structures (see Figure 1). A drawback of the arrangement is that the highly conserved tryptophan W470 in loop 11–12 is pointing out of the active site. It could well be interacting with other subunits of the enzyme and contribute to the electron-transfer path. A comparison of the old and refined models is shown in Figure S1 of the Supporting Information.

Three residues are clearly in different roles in the old and refined models: R471, W470, and Y181. R471 is involved in heme interactions in both models, and functional data on mutatants are not likely to tell the options apart. W470 is hydrogen-bonded to the heme in the old model and assumed to interact with additional subunits in the new model in an unknown way. No experimental data are available for W470, and the agreement to either model cannot be estimated. The third residue with clearly different roles in the two models is Y181. In the old model, it forms a hydrogen bond to W263 (B:W236), and in the refined model, it forms a hydrogen bond to the high-spin heme. The latter role is much more critical, and it is supported by the preliminary data discussed below (Rauhamäki et al., unpublished results).

Active-Site Loops. The interhelical loops 3–4 and 11–12 have been suggested to participate in proton and water exit (*20–22, 25*), and the ionic interactions of loop residues with the hemes modify the midpoint potentials. Accordingly, one of the requirements for molecular models of any terminal oxidase is that all heme propionates participate in polar interactions. In the models, the A-propionate of the low-spin heme interacts with R115 and the Δ-propionate with K179 (see Figure 1). Mutations to a leucine or a methionine would test the importance of these contacts. The high-spin heme A-propionate is bound to N393 and H397 in loop 9–10 in a fully conserved manner. Residues around the Δ-propionate are now arranged in a fashion fully similar to that in the aa_3-type oxidases, with R471 forming an ion pair with the propionate oxygens and Y181 destabilizing it.

The role of the loop 3–4 in proton traffic is puzzling. The loop from the cbb_3-type oxidases is clearly homologous to the nitric oxide reductases (NORs) and not to the aa_3 or ba_3-type oxidases (*8, 9, 34*). Assuming that this is the site of a proton path and knowing that NORs do not pump protons (*35*), it would be tempting to suggest that the cbb_3-type oxidases can take protons from the outside of the cell too.

Mutagenesis has shown that the two conserved glutamates in loop 3–4 (k**E**ya**E**) are both important for activity in NORs (*36*) and the former one in the cbb_3-type oxidases (*12*). In our previous and present models, both acidic residues are in the loop area and thus accessible to either the water medium or other subunits.

Preliminary data on the cbb_3-type oxidase from *R. sphaeroides* show full inactivation on mutations of R471, Y181, and K179 and partial inactivation on mutations of W263 and W264, while the subunit composition and optical absorption spectra of the purified enzymes are unchanged (Rauhamäki et al., unpublished results). The effects seen on mutating K179, Y181, and R471 are in full accordance with their proposed roles as heme counterions in the present model but differ from the effects seen for the same loci in the aa_3-type oxidases. A likely, although not very satisfying explanation, is that the loops 3–4/11–12 are so dissimilar between the two subfamilies, with different subunits around them, that the behavior, too, is to differ. For example, in all enzymes studied by specific point mutations, the destabilizing residue to the arginine−propionate pair is a tryptophan (W164 in *P. denitrificans*), while in many bacterial enzymes, it is a tyrosine. The identity of this loop 3–4 aromatic seems to be coupled to structural features in helix 6, as dicussed in the next section. However, no mutation data are available for these bacterial oxidases. Results for the ba_3-type oxidase from *T. thermophilus* would be most informative.

Helix 6. In the aa_3-type oxidases, helix 6 is indisputably the most central of all helices: over its length of 35 amino acids, 21 are identical from *Paracoccus* to bovine. Four residues are known to be absolutely required for function: B:W236 possibly as a site for a radical (*2, 3*); B:H240 and B:Y244 as the special bidentate Cu_B ligand; and B:E242 as the end point of the D channel. In addition, B:V241 is proposed to act as a steric organizer for O_2 entry (*37*). In the cbb_3-type oxidases, no acidic residues are found in this helix, the tyrosine has moved to the neighboring helix 7, and histidine and valine are at the same sites. However, for the tryptophan, there are now two of them, vicinal and fully conserved. Even for this most conserved helix, alternative alignments can be justified between the structurally known oxidases and the cbb_3-type oxidases that match either of the two tryptophans to the single W in the known structures. The straightforward alignment matches the absolutely conserved histidines (H240/H267 bovine aa_3/*R. sphaeroides* cbb_3) and valines (243/270), which brings W263 of the cbb_3-type oxidases to correspond to the single crucial W of the canonical oxidases. This is what has been presented in all published work thus far (*8, 9, 34, 38*). However, several sequence features imply a gap right after the WW motif in the cbb_3 sequences (see Figure 2), in which case W264 would instead stack to the histidine ligand of Cu_B. First, among non-cbb_3-type oxidases, the dominant motif in helix 6 is fWffgH**P**eVy (residues conserved in the whole superfamily are shown in capital letters, and the discussed proline is shown in bold). For several organisms, though, especially all *Burkholderia*, the sequence motif is sWtlHaiVy. The conserved proline is missing, and there are only two residues between W and H. This is highly suggestive of a proline kink being substituted by underwinding the helix one turn earlier. Insertion of a gap into the cbb_3 sequences is easily justified by the similarly absent proline. A second argument for inserting a gap is presented by the sequence comparison of the ba_3- and cbb_3-type oxidases N-terminal of the WW motif (see Figure 2). A well-conserved site of small amino acids A/S/T of the ba_3-type oxidases aligns with an invariant A of the cbb_3 sequences. In the *Thermus* structure, alanine 224 packs tightly to neighboring residues and the helix is constrained to place by an ionic interaction between the following R225 and D287 from loop 7–8. The contact is found in all sequences with Y in loop 3–4 (Y133 in *T. thermophilus*). Third and most importantly, when comparing models constructed from the two alignments, the gapped G model structure compares better to the known structures in the area above the hemes. In all known structures, there is a clear "ceiling" of tightly packed hydrophobic residues above the active site. In our G model, both tryptophans W263 and W264 participate in an extended cluster of four aromatic residues: H318−W264−W263−Y181 (see Figure 1), packed at van der Waals contacts. In the C model, the corresponding residues are H318−W263−Q262−Y181. The polar glutamine Q262 does not reach to pack tightly to Y181 in any of the models. Bioinformatic arguments thus favor insertion of a gap to helix 6 of the cbb_3-type oxidases.

In the aa_3-type oxidase from *P. denitrificans*, mutation of the helix 6 tryptophan to a phenylalanine renders the enzyme completely inactive (*2*), which has been suggested to be related to radical formation during turnover (*2, 3*). Because mutations of W263 or W264 in the cbb_3-type oxidases show only moderate effects (Rauhamäki et al., unpublished results), it can be concluded that either one tryptophan at a time suffices in this subfamily or no electron depository is needed, and the last electron comes directly from the tyrosine. Data from a double mutant and aliphatic substitutions would be needed to address the question. A third possibility is that the mutational effects of W263, W264, and Y181 in cbb_3-type oxdases are correlated and that the inactivating mutations mechanistically break the same unknown function.

The two alternative models for helix 6, continuous (C) or gapped (G), both agree with the preliminary data. In the C model, the observed effects would arise from the loss of interactions with the histidine ligating Cu_B and nonspecific changes in its interactions with the surroundings. In the G model, we assume that the aromatic "ceiling" connecting Cu_B and high-spin heme Δ-propionate is required for isolating the active site from the highly hydrophilic area above it. In this case, effects reflect the loss of the interaction to Y181 and destabilization of the cluster in a middle position.

His−Tyr Cross-Link. The unique post-translational modification of the heme−copper oxidases, the histidine−tyrosine cross-link, has been predicted and verified to exist in different helices in the oxidase subfamilies (*8–11*). The detailed model allows us to study the structural consequences of the evolutionary migration. Simulations of the bovine oxidase show different average values for the side-chain dihedral angles than those of the cbb_3-type oxidase model, owing to the different position of the Cα of tyrosine. As a result, the tyrosine OH is clearly closer to the high-spin heme iron in the cbb_3 model than in the bovine structure and would directly reach to donate a hydrogen atom to the dioxygen bond to be broken. This stabilizing interaction may be related to the higher oxygen-binding affinity of the cbb_3-type oxidase than that of the aa_3-type oxidase (*39*).

If indeed the cbb_3-type oxidases are evolutionarily more ancient, as the phylogenetic breadth of the data by Hemp et al. (*12*) beautifully implies, the position of the active-site tyrosine in helix 7 should be considered the default and its transfer to helix 6 should be considered a special case. The dynamics simulation of the cbb_3 model suggests that the position of the active-site tyrosine is related to the heme structure: from helix 7, the tyrosine hydroxyl is closer to the metals of the binuclear site and can interact favorably with the substrate. In oxidases with A- or O-type high-spin hemes, the tyrosine hydroxyl is hydrogen-bonded by the hydroxy-ethyl farnesyl chain, which stabilizes the side chain to a gauche−minus configuration.

Definition of the cbb_3-Type Oxidases. In the sequence analysis of the cbb_3-type oxidases by Hemp et al. (*12*), all residues discussed here are claimed not to be conserved. This demands discussion. The data set used is remarkably large, including 246 cbb_3 sequences from various genomic projects. The sequence features defining the subfamily are not explained. We analyzed their data in Figure S1 of the Supporting Information and find that the functionally characterized cbb_3-type oxidases from *B. japonicum*, *R. sphaeroides*, *R. capsulatus*, and *V. cholerae* form a tight mutually similar group, where all pairwise identities are over 60%. We consider this central set to be the correct comparison set for interpolating sequence motifs for mechanistic proposals.

Analysis of the large sequence alignment of Hemp et al. (*12*) reveals several other features. Clearly, sequences from 202 to 223 form a phylogenetically closed set, because all oxidase sequences from the order *Campylobacterales* cluster together here (see Figure 3). It is also worth mentioning that for many organisms, e.g., *Silicibater pomeroyi* and *Photobacter profundum*, there are two different sequences from the same strain, one of which belongs to the central set, while the other lacks the loop 11–12 arginine (R471 *R. sphaeroides* cbb_3). We consider that both of these features, clustering according to bacterial phylogeny and alternative oxidases found from the same organisms, strengthen our definition of the central set as mechanistically unified. In this case, the variant cbb_3-like sequences might well represent another subfamily with varying subunit composition and perhaps with less efficient or absent proton-pumping, being oxygen scavengers as the NO reductases. For a comparison, the sequence identities between three different terminal oxidases from *P. denitrificans* are $aa_3/cbb_3 = 21\%$, aa_3/NOR = 17%, and cbb_3/NOR = 21%.

The nonconservancy of the active-site residues even in the selected smaller set of well-conserved cbb_3-type oxidases is puzzling, especially for the loop 11–12 arginine (R471). The demand of identical residues is not necessarily relevant though, because it is often seen in mutation experiments that the same functional role can be served by several different amino acids, with changed activity. For example, in the *E. coli* bo_3-type oxidase, the arginine in loop 11–12 that forms an ion pair with the propionate can be substituted by a Q. If we assume that the cbb_3-type oxidases are equally tolerant, we are still left with six leucines and four serines as the aberrant residues at the position. The former are from *Psychrobacters*, living in extremely cold and saline environments, and the latter are from the pathogen *Neisseria*. Multiple occurrence and phylogenetic grouping speak against sequencing errors. Still, both leucine and serine differ from arginine at the codon level by one base only.

CONCLUSIONS

Present-day huge amounts of nucleotide data are valuable in analyzing evolutionary relationships but utmost caution is required in interpreting the data in structural and functional terms. Clearly, nucleotide sequence data and functional enzymatic data do not define the cbb_3-type oxidases in the same way.

Updated homology models of the active site of the cbb_3-type oxidase from *R. sphaeroides* were constructed to agree with all available data, and they show remarkably similar interactions of the high-spin heme in the different oxidase subfamilies. A possibly important structural feature isolating the hydrophobic active site and the hydrophilic output area has been identified and modeled.

ACKNOWLEDGMENT

We thank Dr. Anne Puustinen for her continuous help and critical reading of the manuscript, Ms. Virve Rauhamäki for access to unpublished data, and Mr. Ben Webb for generous help with the Modeller program.

SUPPORTING INFORMATION AVAILABLE

A figure comparing the refined model to the old model, as described in the text. This material is available free of charge via the Internet at http://pubs.acs.org.

REFERENCES

1. Proshlyakov, D. A., Pressler, M. A., DeMaso, C., Leykam, J. F., DeWitt, D. L., and Babcock, G. T. (2000) Oxygen activation and reduction in respiration: Involvement of redox-active tyrosine 244. *Science 290*, 1588–1591.
2. MacMillan, F., Budiman, K., Angerer, H., and Michel, H. (2006) The role of tryptophan 272 in the *Paracoccus denitrificans* cytochrome *c* oxidase. *FEBS Lett. 580*, 1345–1349.
3. Wiertz, F. G., Richter, O. M., Ludwig, B., and de Vries, S. Kinetic resolution of a tryptophan-radical intermediate in the reaction cycle of *Paracoccus denitrificans* cytochrome *c* oxidase, *J. Biol. Chem.* 2007, in press.
4. Ferguson-Miller, S., and Babcock, G. T. (1996) Heme/copper terminal oxidases. *Chem. Rev. 96*, 2889–2907.
5. Hosler, J. P., Ferguson-Miller, S., and Mills, D. A. (2006) Energy transduction: Proton transfer through the respiratory complexes. *Annu. Rev. Biochem. 75*, 165–187.
6. Toledo-Cuevas, M., Barquera, B., Gennis, R. B., Wikström, M., and Garcia-Horsman, J. A. (1998) The cbb_3-type cytochrome *c* oxidase from *Rhodobacter sphaeroides*, a proton-pumping heme−copper oxidase. *Biochim. Biophys. Acta 1365*, 421–434.
7. Zufferey, R., Preisig, O., Hennecke, H., and Thöny-Meyer, L. (1996) Assembly and function of the cytochrome cbb_3 oxidase subunits in *Bradyrhizobium japonicum*. *J. Biol. Chem. 271*, 9114–9119.
8. Hemp, J., Christian, C., Barquera, B., Gennis, R. B., and Martinez, T. J. (2005) Helix switching of a key active-site residue in the cytochrome cbb_3 oxidase. *Biochemistry 44*, 10766–10775.
9. Sharma, V., Puustinen, A., Wikström, M., and Laakkonen, L. (2006) Sequence analysis of the cbb_3 oxidases and an atomic model for the *Rhodobacter sphaeroides* enzyme. *Biochemistry 45*, 5754–5765.
10. Rauhamäki, V., Baumann, M., Soliymani, R., Puustinen, A., and Wikström, M. (2006) Identification of a histidine−tyrosine cross-link in the active site of the cbb_3-type cytochrome *c* oxidase from *Rhodobacter sphaeroides*. *Proc. Natl. Acad. Sci. U.S.A. 103*, 16135–16140.
11. Hemp, J., Robinson, D. E., Ganesan, K. B., Martinez, T. J., Kelleher, N. L., and Gennis, R. B. (2006) Evolutionary migration of a post-translationally modified active-site residue in the proton-

pumping heme−copper oxygen reductases. *Biochemistry 45*, 15405–15410.
12. Hemp, J., Han, H., Roh, J. H., Kaplan, S., Martinez, T. J., and Gennis, R. B. (2007) Comparative genomics and site-directed mutagenesis support the existence of only one input channel for protons in the C-family (*cbb*$_3$ oxidase) of heme−copper oxygen reductases. *Biochemistry 46*, 9963–9972.
13. Ostermeier, C., Harrenga, A., Ermler, U., and Michel, H. (1997) Structure at 2.7 Å resolution of the *Paracoccus denitrificans* two-subunit cytochrome *c* oxidase complexed with an antibody Fv fragment. *Proc. Natl. Acad. Sci. U.S.A. 94*, 10547–10553.
14. Soulimane, T., Buse, G., Bourenkov, G. P., Bartunik, H. D., Huber, R., and Than, M. E. (2000) Structure and mechanism of the aberrant *ba*$_3$ cytochrome *c* oxidase from *Thermus thermophilus*. *EMBO J. 19*, 1766–1776.
15. Abramson, J., Riistama, S., Larsson, G., Jasaitis, A., Svensson-Ek, M., Laakkonen, L., Puustinen, A., Iwata, S., and Wikström, M. (2000) The structure of ubiquinol oxidase from *Escherichia coli*. *Nat. Struct. Biol. 7*, 910–917.
16. Svensson-Ek, M., Abramson, J., Larsson, G., Tornroth, S., Brezezinski, P., and Iwata, S. (2002) The X-ray crystal structures of wild-type and EQ(I-286) mutant cytochrome *c* oxidases from *Rhodobacter sphaeroides*. *J. Mol. Biol. 321*, 329–339.
17. Tsukihara, T., Shimokata, K., Katayama, Y., Shimada, H., Muramoto, K., Aoyama, H., Mochizuki, M., Shinzawa-Itoh, K., Yamashita, E., Yao, M., Ishimura, Y., and Yoshikawa, S. (2003) The low-spin heme of cytochrome *c* oxidase as the driving element of the proton-pumping process. *Proc. Natl. Acad. Sci. U.S.A. 100*, 15304–15309.
18. Qin, L., Hiser, C., Mulichak, A., Garavito, R. M., and Ferguson-Miller, S. (2006) Identification of conserved lipid/detergent-binding sites in a high-resolution structure of the membrane protein cytochrome *c* oxidase. *Proc. Natl. Acad. Sci. U.S.A. 103*, 16117–16122.
19. Shinzawa-Itoh, K., Aoyama, H., Muramoto, K., Kurauchi, T., Mizushima, T., Yamashita, E., Tsukihara, T., and Yoshikawa, S. (2007) Structures and physiological roles of 13 integral lipids of bovine heart cytochrome *c* oxidase. *EMBO J. 26*, 1713–1725.
20. Puustinen, A., and Wikström, M. (1999) Proton exit from the heme−copper oxidase of *Escherichia coli*. *Proc. Natl. Acad. Sci. U.S.A. 96*, 35–37.
21. Qian, J., Mills, D. A., Geren, L., Wang, K., Hoganson, C. W., Schmidt, B., Hiser, C., Babcock, G. T., Durham, B., Millett, F., and Ferguson-Miller, S. (2004) Role of the conserved arginine pair in proton and electron transfer in cytochrome *c* oxidase. *Biochemistry 43*, 5748–5756.
22. Ribacka, C., Verkhovsky, M. I., Belevich, I., Bloch, D. A., Puustinen, A., and Wikström, M. (2005) An elementary reaction step of the proton pump is revealed by mutation of tryptophan-164 to phenylalanine in cytochrome *c* oxidase from *Paracoccus denitrificans*. *Biochemistry 44*, 16502–16512.
23. Budiman, K., Kannt, A., Lyubenova, S., Richter, O. H., Ludwig, B., Michel, H., and MacMillan, F. (2004) Tyrosine 167: The origin of the radical species observed in the reaction of cytochrome *c* oxidase with hydrogen peroxide in *Paracoccus denitrificans*. *Biochemistry 43*, 11709–11716.
24. Wikström, M., Verkhovsky, M. I., and Hummer, G. (2003) Water-gated mechanism of proton translocation by cytochrome *c* oxidase. *Biochim. Biophys. Acta 1604*, 61–65.
25. Wikström, M., Ribacka, C., Molin, M., Laakkonen, L., Verkhovsky, M., and Puustinen, A. (2005) Gating of proton and water transfer in the respiratory enzyme cytochrome *c* oxidase. *Proc. Natl. Acad. Sci. U.S.A. 102*, 10478–10481.
26. Sali, A., and Blundell, T. L. (1993) Comparative protein modeling by satisfaction of spatial restraints. *J. Mol. Biol. 234*, 779–815.
27. Humphrey, W., Dalke, A., and Schulten, K. (1996) VMD−Visual Molecular Dynamics. *J. Mol. Graph. 14*, 33–38.
28. Thompson, J. D., Gibson, T. J., Plewniak, F., Jeanmougin, F., and Higgins, D. G. (1997) The ClustalX windows interface: Flexible strategies for multiple sequence alignment aided by quality analysis tools. *Nucleic Acids Res. 25*, 4876–4882.
29. Hall, T. A. (1999) BioEdit: A user-friendly biological sequence alignment editor and analysis program for Windows 95/98/NT. *Nucleic Acids Symp. Ser. 41*, 95–98.
30. Zhang, L., and Hermans, J. (1996) Hydrophilicity of cavities in proteins. *Proteins 24*, 433–438.
31. Kalé, L., Skeel, R., Bhandarkar, M., Brunner, R., Gursoy, A., Krawetz, N., Phillips, J., Shinozaki, A., Varadarajan, K., and Schulten, K. (1999) NAMD2: Greater scalability for parallel molecular dynamics. *J. Comput. Phys. 151*, 283–312.
32. MacKerell, A. D., Jr., Bashford, D., Bellott, M., Dunbrack, R. L., Jr., Evanseck, J. D., Field, M. J., Fischer, S., Gao, J., Guo, H., Ha, S., Joseph-McCarthy, D., Kuchnir, L., Kuczera, K., Lau, F. T. K., Mattos, C., Michnick, S., Ngo, T., Nguyen, D. T., Prodhom, B., Reiher, W. E., III, Roux, B., Schlenkrich, M., Smith, J. C., Stote, R., Straub, J., Watanabe, M., Wiorkiewicz-Kuczera, J., Yin, D., and Karplus, M. (1998) All-atom empirical potential for molecular modeling and dynamics studies of proteins. *J. Phys. Chem. B 102*, 3586–3616.
33. Johansson, M. P., Kaila, V. R. I., and Laakkonen, L. Charge parameterization of the metal centers in cytochrome *c* oxidase, *J. Comput. Chem.* 2007, in press.
34. Hendriks, J., Gohlke, U., and Saraste, M. (1998) From NO to OO: Nitric oxide and dioxygen in bacterial respiration. *J. Bioenerg. Biomembr. 30*, 15–24.
35. Zumft, W. G. (1997) Cell biology and molecular basis of denitrification. *Microbiol. Mol. Biol. Rev. 61*, 533–616.
36. Thorndycroft, F. H., Butland, G., Richardson, D. J., and Watmough, N. J. (2007) A new assay for nitric oxide reductase reveals two conserved glutamate residues form the entrance to a proton conducting channel in the bacterial enzyme. *Biochem. J. 401*, 111–119.
37. Riistama, S., Puustinen, A., Verkhovsky, M. I., Morgan, J. E., and Wikström, M. (2000) Binding of O_2 and its reduction are both retarded by replacement of valine 279 by isoleucine in cytochrome *c* oxidase from *Paracoccus denitrificans*. *Biochemistry 39*, 6365–6372.
38. Pereira, M. M., Santana, M., and Teixera, M. (2001) A novel scenario for the evolution of haem−copper oxygen reductases. *Biochim. Biophys. Acta 1505*, 185–208.
39. Preisig, O., Zufferey, R., Thöny-Meyer, L., Appelby, C. A., and Hennecke, H. (1996) A high-affinity *cbb*$_3$-type cytochrome *c* oxidase terminates the symbiosis-specific respiratory chain of *Bradyrhizobium japonicum*. *J. Bacteriol. 178*, 1532–1538.

BI702088R